JOURNAL OF CATALYSIS 24, 130–145 (1972)

The Nature of Raney Nickel

VI. Transmission and Scanning Electron Microscopy Studies

S. D. ROBERTSON,* J. FREEL,† AND R. B. ANDERSON

Department of Chemical Engineering and Institute for Materials Research, McMaster University, Hamilton, Ontario, Canada

Received April 5, 1971

Various preparations of Raney nickel were examined by transmission electron microscopy but the scope of this study was limited by catalyst instability in the electron beam under normal operating conditions. Different approaches to overcome this problem were made and interpretable results were obtained with low electron beam irradiation of the specimen. No particular shape was observed in the catalyst grains and neither was there, in general, a preferred orientation of the nickel crystallites. Alumina trihydrates were identified by electron diffraction, but the presence of γ and other aluminas suggested that dehydration occurs in the microscope.

Topographical studies with the scanning electron microscope on alumina trihydrate-rich Raney nickel have shown that the trihydrate is in the form of a crystalline deposit covering most of the catalyst surface. This interpretation was confirmed by electron-probe microanalysis. The surface topography of "completely activated" catalysts revealed the presence of particles, presumably alumina trihydrate, in or near fissures in the Raney nickel.

INTRODUCTION

The composite nature of the Raney nickel catalyst, found by X-ray diffraction studies (*1–3*), has been the subject of little study by electron microscopy. However, Yasamura (*4*) has reported that fresh catalyst particles have a pyramidal shape based on their morphology in the electron microscope. Knappwost and Mader (*5*), in a similar study, reported that the catalyst exists as sponge-like macroparticles composed of nickel particles in a support which was amorphous in structure. The volume and form of these macroparticles was determined by the particle size of the finely ground initial alloy and the nickel crystallites in all cases showed a preferred [110] texture.

As part of a wider investigation of the properties of this catalyst (*6–8*), it seemed pertinent to examine the fine structure of particulate Raney nickel by transmission microscopy and electron diffraction. Adsorption and X-ray diffraction studies of various catalyst preparations have shown that marked structural differences can result from different activation conditions (*3, 6*). To obtain further information on these factors, surface topographical studies were made using the scanning electron microscope, the principles (*9, 10*) and applications (*11, 12*) of which have been reported.

EXPERIMENTAL METHODS

The preparation of Raney nickels and the nomenclature used to describe them has been discussed previously (*6*). Because of the pyrophoric nature of the catalyst, care was taken to preclude air oxidation during their preparation for electron micros-

* Present address: Afdeling F. R./Koninklijke/ Shell-Laboratorium Amsterdam, Badhuisweg 3, Amsterdam-N, The Netherlands.

† Present address: Gulf Research and Development Co., Drawer 2038, Pittsburgh, Pa. 15230.

copy. To this end, specimens were ground under ethanol and then suspended in a 2% nitrocellulose solution prior to dispersion over a clean glass slide. A thin carbon coating was evaporated onto this film after drying *in vacuo*. The composite was then cleaved off onto a distilled water surface and the film transferred to copper grids on a fine stainless-steel mesh.

A Philips E. M. 300 transmission electron microscope was used to investigate the fine structure of the catalysts. Information on the composition of various components was obtained from selected area diffraction and the magnitude of catalyst crystalline domain sizes was studied by the high-resolution dark-field technique, the principles of which have been fully discussed (*13*) and its various applications to catalyst structures have been reported (*14*, *15*). To minimize the thermal effects of electron beam irradiation, specimens were cooled in the vacuum of the instrument to about —140°C between the blades of a cold finger maintained at —195°C, the latter preventing hydrocarbon vapor contamination of the samples (*16*). Such cooling techniques, however, caused residual isoamyl to freeze out over the specimen, rendering it useless for microscopy. Consequently, Raney nickel was dispersed over carbon films with the bulk of the ethanol medium being removed in the vacuum of the microscope prior to specimen cooling. No changes in the support structure was found but high index NiO reflections were present in the catalyst diffraction patterns. Useful data was only obtained with low electron beam intensities under an acceleration voltage of 100 kV.

For scanning electron microscopy, Raney nickel specimens were dispersed in a 2% nitrocellulose solution over mushroom-shaped specimen mounts. An aluminum film was evaporated on to this dispersion

FIG. 1. Transmission electron micrographs (Figs. 1–9): Catalyst specimen from $IIIA_2$ preparation after initial exposure to the electron beam; 16,000×.

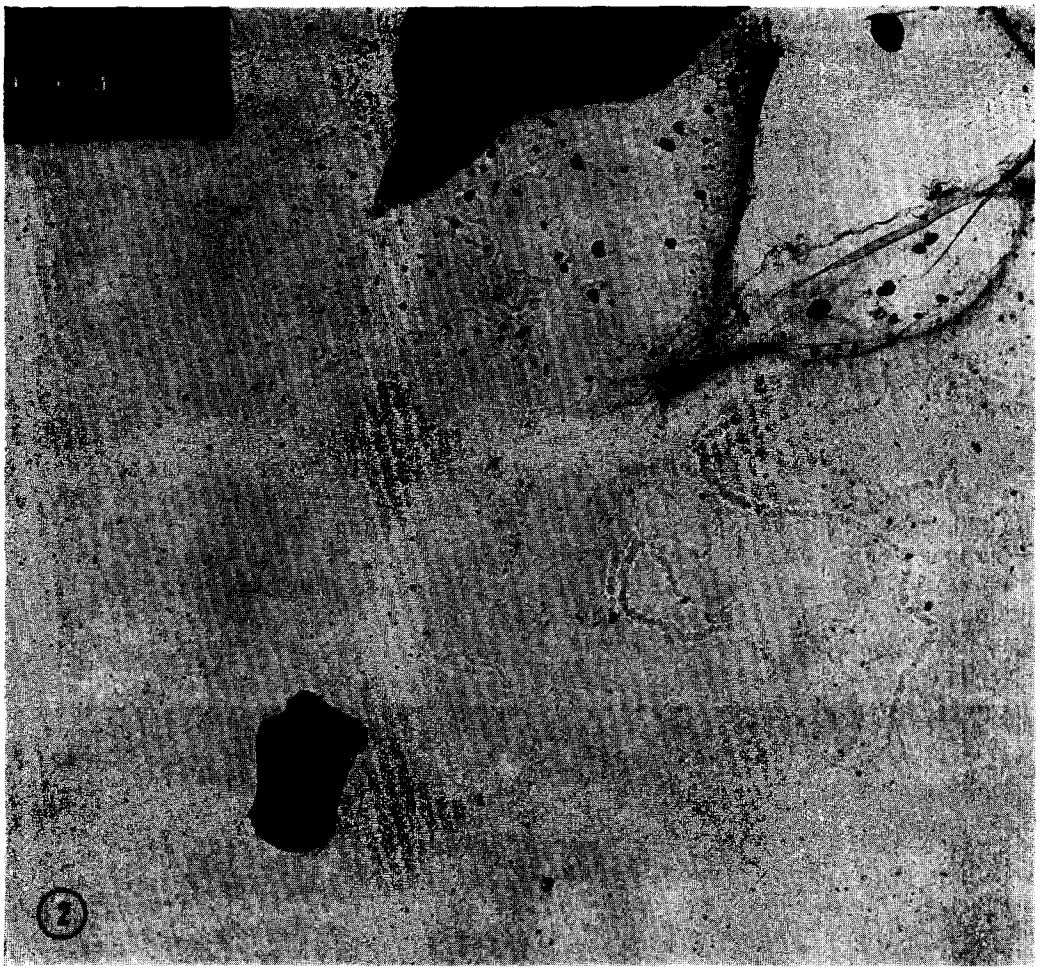

FIG. 2. Specimen in Fig. 1 after sintering under slightly more intense electron beam irradiation: Dispersion of small particles formed by diffusion from the main catalyst specimen; 13,000×.

after drying to enable the efficient electrical conduction required for surface topography study in the Stereoscan Mark IIA scanning electron microscope.

RESULTS

One of the main problems in a conventional transmission electron microscope study of Raney nickel is illustrated in Figs. 1 and 2 where the former is a typical $IIIA_2$ catalyst particle that has just been exposed to the electron beam irradiation. On focusing the beam somewhat more closely on to the specimen the effects of Fig. 2 are observed. The daughter particles were observed to have diffused away from the parent mass (diffusion channels along the background film giving evidence of this process) and a selected area electron diffraction pattern (Fig. 3) reflected the very highly crystalline nature of these particles—a feature not in keeping with X-ray diffraction properties of Raney nickel (*3*).

Similar problems attend an electron microscopy examination of the nature of the alumina trihydrate by-products in various preparations. The flaky specimen in Fig. 4 gives a selected area diffraction pattern on Fig. 5 which is a composite of boehmite ($Al_2O_3 \cdot 3H_2O$) and γ-alumina (γAl_2O_3)—that is a mixture of hydrated and dehydrated aluminas. Selected area

FIG. 3. Selected area diffraction fraction from a group of such small particles that are formed by this diffusion process.

diffraction patterns corresponding to other dehydrated aluminas were also found—a resultant by-product structure that is considered unlikely in view of the low temperature aqueous catalyst preparation (*17*). It is suggested that the vacuum and electron beam conditions of the microscope engenders dehydration and structural changes of the original trihydrate specimens.

One way of minimizing electron beam induced changes in the structure of the catalyst and its by-products is to examine specimens at very low levels of radiation intensity. Despite viewing difficulties some more meaningful data can be produced. For example, Fig. 7 corresponds to a selected area diffraction pattern from part of the specimen in Fig. 6. The spot row pattern arising from the more massive rectangular and triangular components of the specimen, corresponds to bayerite while the ring pattern comes from boehmite. Such an occurrence of two alumina trihydrate species in the IIA + 4 hr/100°C/H_2O treated sample would seem to be in accord with the equilibrium of alumina trihydrate structures reported for such temperatures (*18*).

A thin edge area of typical $IIIA_2$ Raney nickel specimen, imaged under low electron beam intensity conditions, gave the diffraction pattern on Fig. 8. Small arcs from the innermost (111) and (200) reflections were displaced under the objective aperture centered on the optical axis of the microscope. The dark-field picture resulting from the diffracted beams in such a chosen segment being used as the imaging radiation is shown in Fig. 9. In the general dark background of the specimen there are

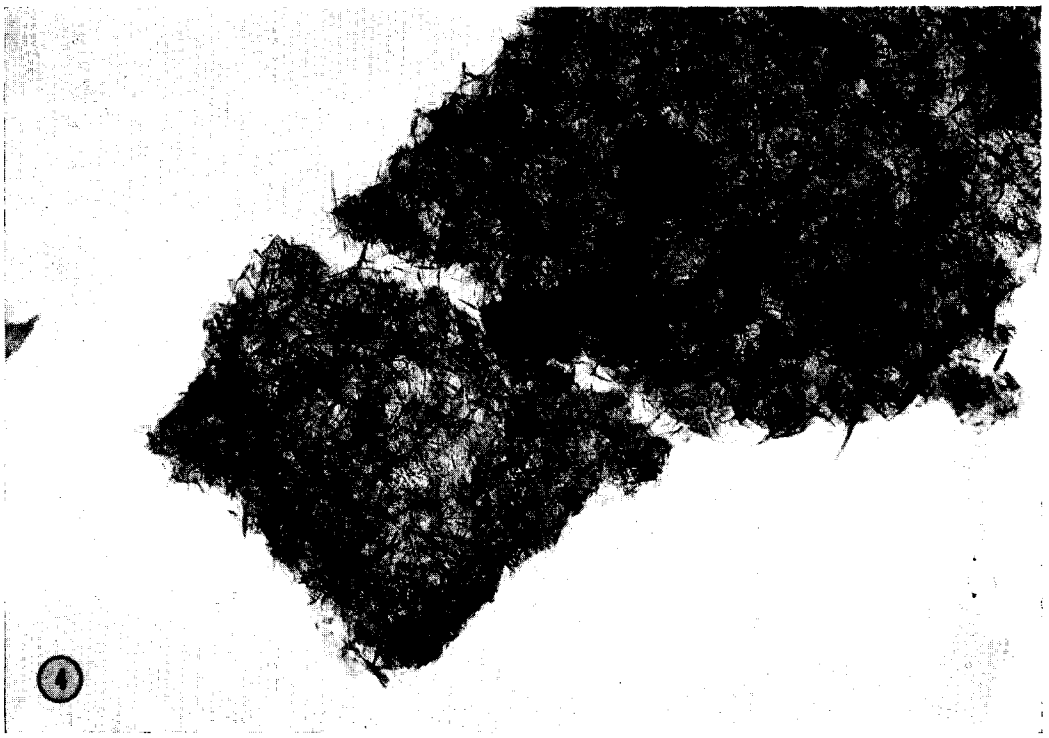

FIG. 4. Platelet specimen from the Type IIA + 4 hr/100°C/H_2O preparation; 52,000×.

many bright domains—denoting crystalline zones in the catalyst that are responsible for the selected diffracted beams. The sizes of completely discernible domain regions (ranged from 40 to 150 Å) of this catalyst compared with the crystallite size from X-ray data of 52 Å (*3*).

Figures 10 to 12 show various areas of the IVA type of catalyst as viewed in the scanning electron microscope. This catalyst was activated by using less than the stoichiometric amount of alkali and contains a large concentration of alumina trihydrate.

The micrographs are interpreted as showing crystalline alumina trihydrate deposited on particles of Raney nickel. The morphology of this layer over the nickel surface closely resembles aluminas reported in a scanning electron microscopy study of multicomponent catalysts (*12*). Further evidence of the aluminum-rich nature of this layer and of the diminished exposure of the nickel areas was obtained from scanning type IVA specimens under the electron beam of an "Acton" electron-probe microanalyzer. Quartz and mica analyzing crystals were used to obtain the nickel and aluminum K-α reflections, respectively. A typical scan over a type IVA grain is shown in Fig. 13. On scanning from point A to point B (a distance of about 120 μ over the surface of the grain shown) nickel and aluminum K_α emissions were recorded as shown. Clearly, there is a sharp division of nickel and aluminum over the specimen surface as a maximum signal in one element corresponds to a minimum in the other. Similar signal variations were obtained when the probe beam was scanned over other grains of the IVA catalyst. Unfortunately, only qualitative information on the distribution of nickel and aluminum can be obtained from this technique due to roughness of the particles interfering with both the quantity of X-ray intensity that can be detected and also the electron current from the specimen. The latter is used to obtain the electron image of the specimen and the

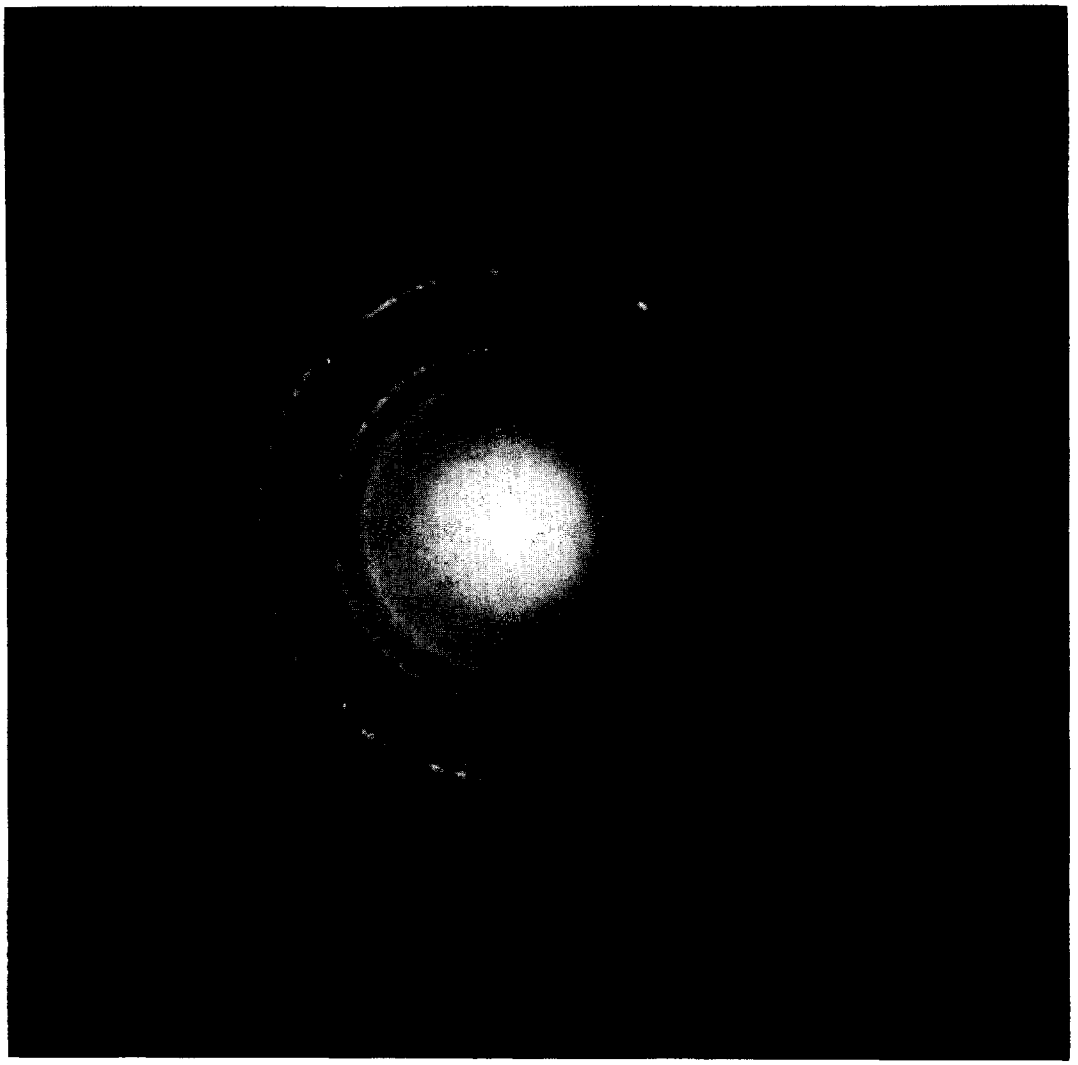

FIG. 5. Selected area diffraction pattern from platelet specimen in Fig. 4: Actual area giving pattern shown in the inset and the pattern corresponds to a mixture of boehmite ($Al_2O_3 \cdot 3H_2O$) and γ-alumina (Al_2O_3).

poor resolution of the picture shown is also contributed to by the nitrocellulose matrix which protects the catalyst from atmospheric oxidation.

Those nickel catalyst areas that are exposed below the covering skin show many fissures. These are "decorated" with lath-like crystallites as shown, for example, in Fig. 11 and is illustrative of the trapping properties of such features. Their ability to bridge and presumably block cracks about 2 μ wide is shown in Fig. 12.

Alkali treatment of the IVA catalyst increased its surface area and pore volume, and X-ray data and chemical analyses indicated that this change was accompanied by a decrease in the concentration of alumina trihydrate (*3*). This effect is also found in the scanning electron pictures displayed on Figs. 14 and 15. Some of the catalyst particles retain the trihydrate cover (Fig. 14) but its highly crystalline appearance is not maintained here. These results could be due to partial dissolution of the alumina. Others, however, as shown in Fig. 15, for example, reveal nickel areas

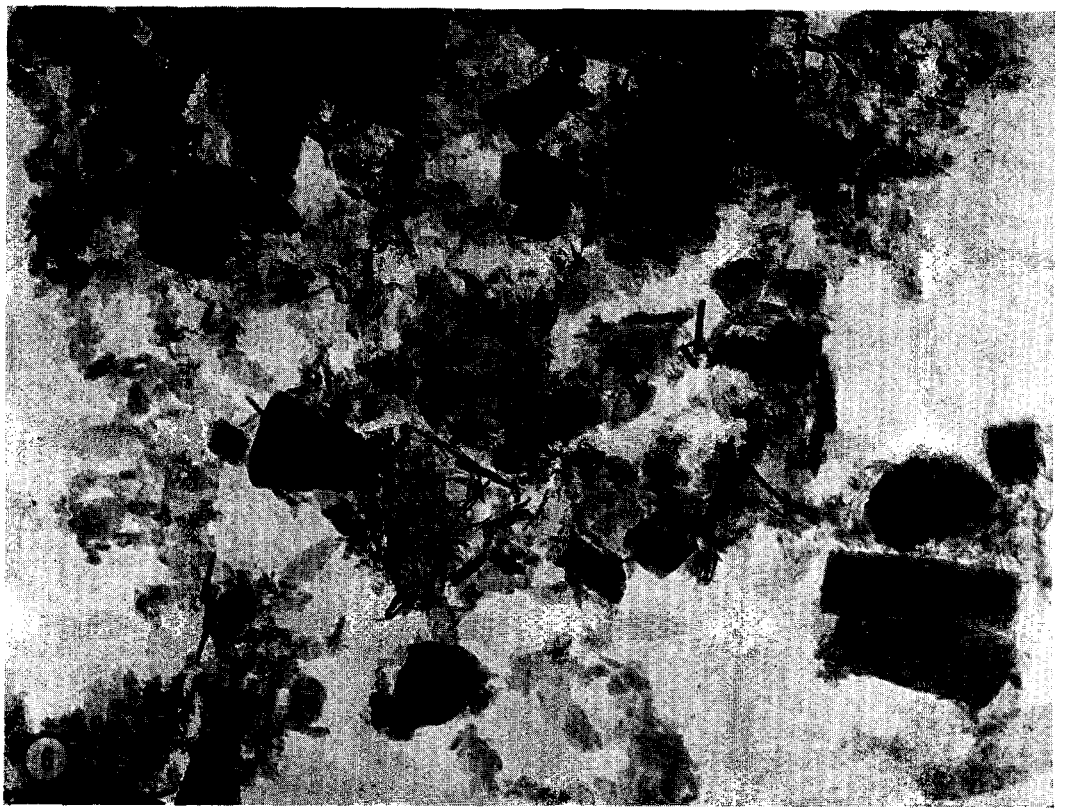

FIG. 6. Alumina trihydrate specimen, showing dark tabloid and light flake features, from Type IIA + 4 hr/100°C/H_2O preparation; 52,000×.

from which most of the alumina trihydrate has been removed. Here greater area of nickel was exposed for adsorption consistent with the larger surface area and porosity of this preparation in contrast to the parent IVA type (*3*).

Figures 16 and 17, for a IIA catalyst prepared with excess alkali, also showed less alumina on the particles. The alumina-free areas had numerous cracks which could result from bulk volume contraction of the alloy during the leaching process (*7*). Fissure widths on Fig. 17 vary from around 1000 Å to 2 μ with a larger proportion of those in the smaller size range. An interesting feature of these fissures is the association of foreign particulate material with them. These particles are probably by-products of the extracted process—such as alumina trihydrates. Identification of the chemical nature of these particles could not, however, be obtained with available instruments.

The surface topography of the IIA_1 catalyst type, as shown in Figs. 18 and 19, resembles that of the Type IIA in that there are extensive nickel particle areas available for adsorption (in contrast to IVA) with particulate residues being confined to crack and wide channel areas. As this catalyst type is also "completely activated" the particulate areas are most probably due to alumina trihydrate. The fissures in $IIIA_1$ are, in general, much wider than in the Type IIA. This effect could be a function of more severe leaching conditions and the consequent sintering of the catalyst (*3*).

DISCUSSION

These studies largely confirm the X-ray diffraction data of previous workers (*1–3*) showing that the two predominant crystalline phases in Raney nickel phase itself and alumina trihydrate. In addition, smaller amounts of aluminas other than

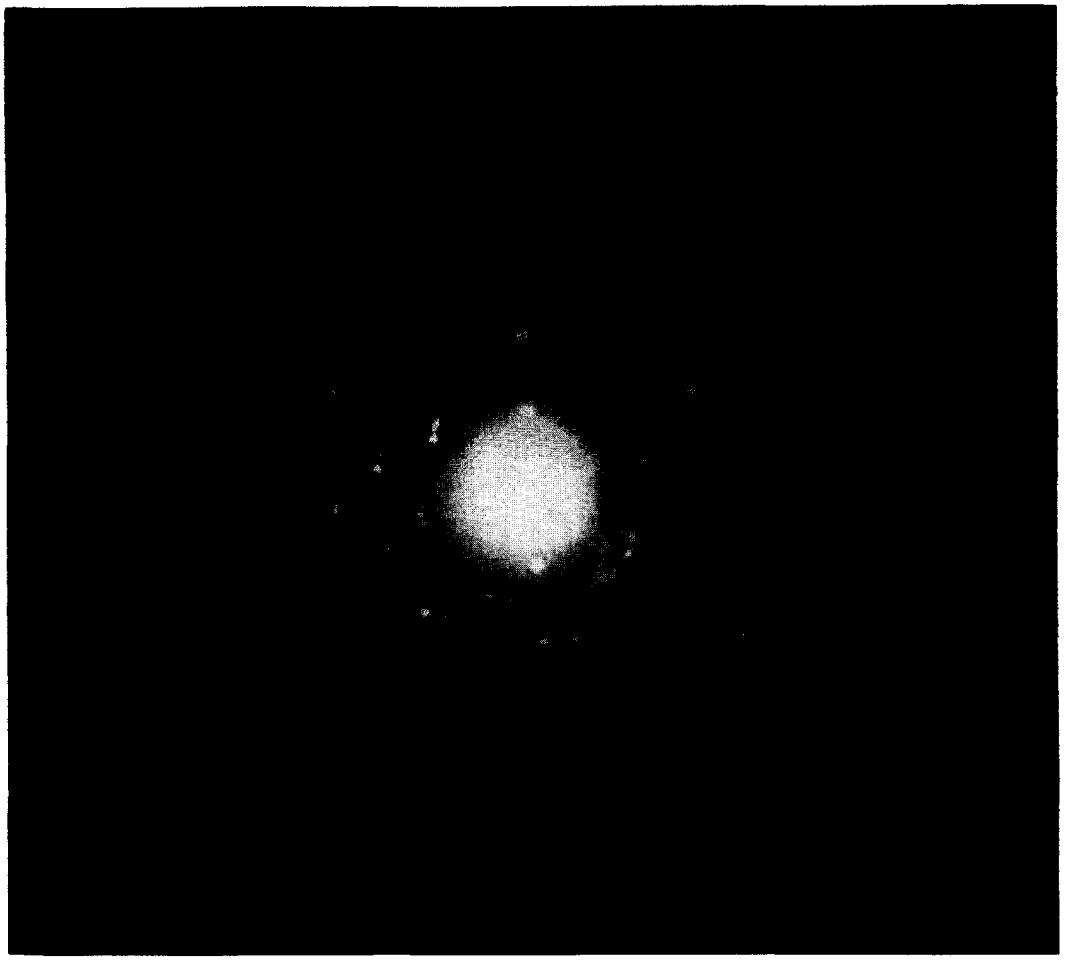

FIG. 7. Composite selected area diffraction pattern from area (in inset) of specimen in Fig. 6. Spot row pattern corresponds to bayerite while the ring pattern corresponds to boehmite.

bayerite have been detected. Much of the alumina is in the form of discrete particles separate from the nickel phase, suggesting the precipitation of alumina from the aqueous solutions obtained during extraction and washing.

These observations on the distinct separation of nickel and alumina phases appear to be contrary to those of Knappwost and Mader (*5*) but the grinding methods used in specimen preparation for electron microscopy could account for this. Diffraction patterns obtained from the nickel particles showed no evidence of reflections other than the nickel phase itself. Much of the alumina content of the catalyst, therefore, seems to be in the form of discrete, microscopic particles. This conclusion is consistent with the high fraction of the total surface area which is nickel metal (*2*, *8*). Most of the Raney nickel catalysts did not show any marked preferred orientation of their crystallites but some selected area diffraction patterns, similar to those observed by other workers (*5*), did display marked texture effects. The reasonable agreement between crystallite sizes from the high resolution dark-field and X-ray line broadening methods suggests the usefulness of further work in this direction. There was no particular shape or form to the Raney nickel particles observed here and from a

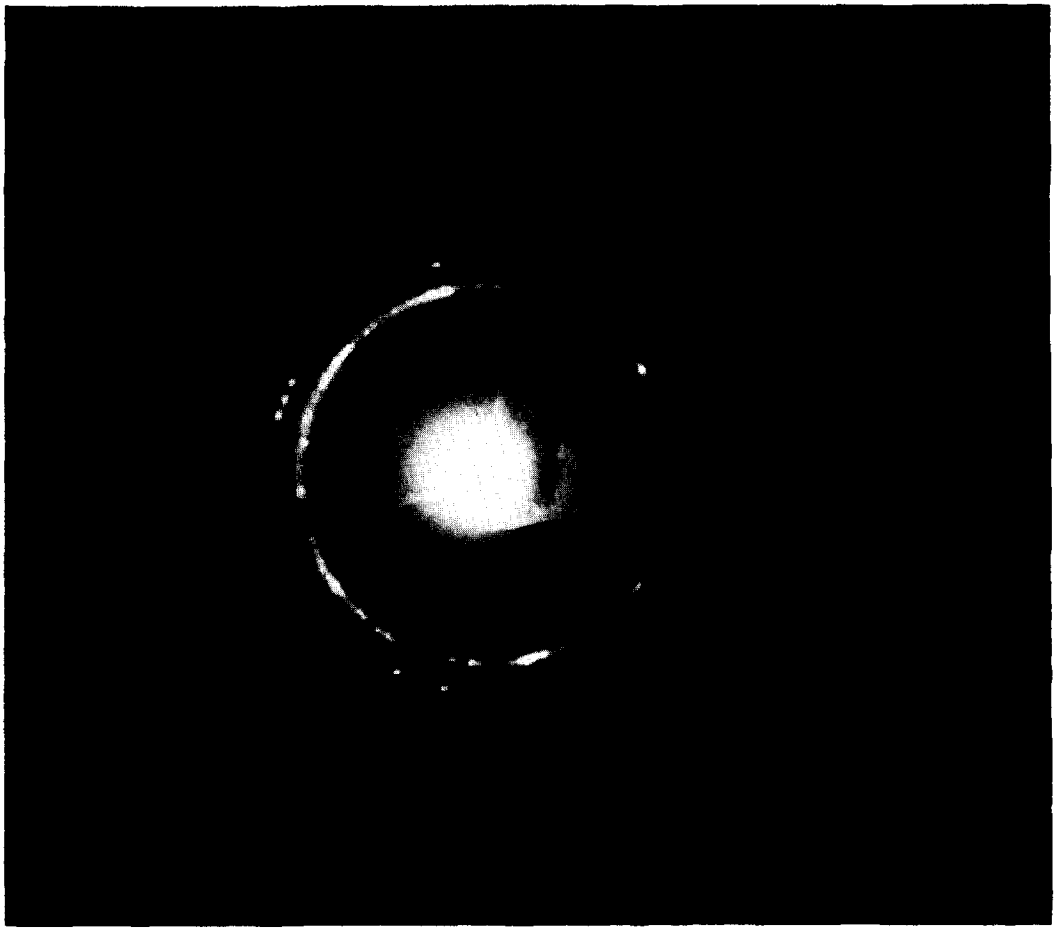

FIG. 8. Selected area diffraction pattern (under low electron beam intensities) of thin edge area in Type $IIIA_1$ specimen of Raney nickel. Area giving the pattern is in the inset.

comparison of the micrographs of Yasumura (*4*) with those of the present study and with those of bayerite given by Lippens (*17*), it seems possible that the pyramidal particles observed by Yasumura and identified as Raney nickel, were really alumina trihydrate.

The scope of transmission electron microscopy in the present study of Raney nickel has been severely limited by specimen instability in the electron beam when the instrument is used under normal operating conditions. Recrystallization of other nickel catalysts under the electron beam has been reported by Coenen (*19*) and this thermal effect could also be responsible for the uncertainty found in the characterization by selected area electron diffraction of the alumina trihydrate. Identification of many of these proved impossible because of their amorphous properties or reflections that could not be correlated to any known diffraction pattern. These difficulties would arise from trihydrate dehydration under vacuum heating of the electron beam and such limitations in the electron microscopy of trihydrates has been reported by Lippens (*17*). Low beam currents reduced greatly the heating effects on the specimens but viewing and recording difficulties were considerable. Image intensifier devices have been developed for transmission electron

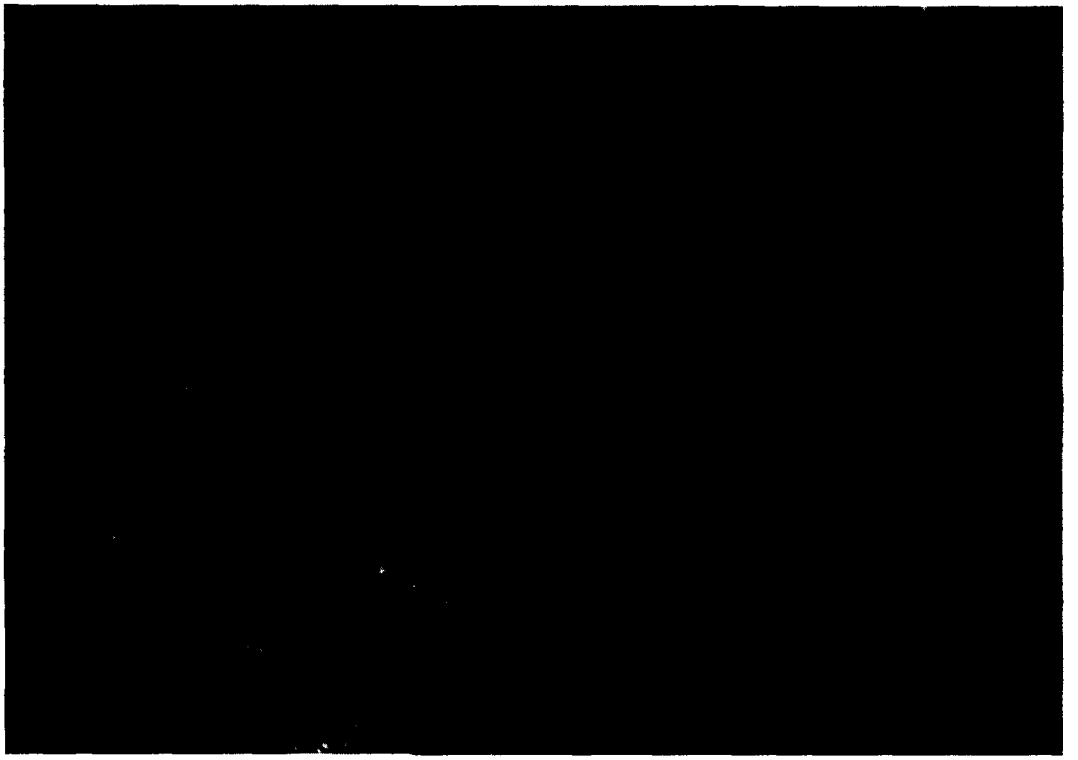

FIG. 9. Dark-field image, from some of the (111) and (200) diffracted beams in Fig. 8 being used as the imaging radiation; 31,500×.

microscopy (*20*) which could ameliorate this probelm.

The electrical and thermal conductivity of the aluminum film that covers the Raney nickel catalysts for scanning electron microscopy could be responsible for the far greater specimen stability in the electron beam. No changes were observed in surface topography during specimen irradiation and interpretable data could be obtained.

The scanning electron microscope, however, while eliminating replication problems associated with contoured surfaces, has a limited resolution value of around 500 Å and any fine pore structural detail, as given by adsorption data, for example, will not be revealed. Consequently, it can be applied only to general topographical interpretation and little insight into the fine structure of catalyst particles can be obtained. However, the method does furnish very useful information especially on the nature of the alumina trihydrate in Type IVA catalyst.

X-Ray (*3*) and electron diffraction evidence has suggested that part or all of the alumina trihydrate is highly crystalline. The surface morphology of the IVA catalyst as shown in these scanning electron pictures emphasises most vividly the highly angular topography of the outer skin that covers most of the catalyst particles. This extensive and crystalline nature of the covering layer over the catalyst grains is good evidence for the suggestion from adsorption data (*6*) that the alumina trihydrate functions as a low area, pore blocking species for gas adsorption on this catalyst type. The blocking effect of residual trihydrate in large pores of Raney nickel and the effect of alkali in exposing fresh nickel areas for adsorption is also shown in the scanning electron micrographs of other catalysts. This is in keeping with

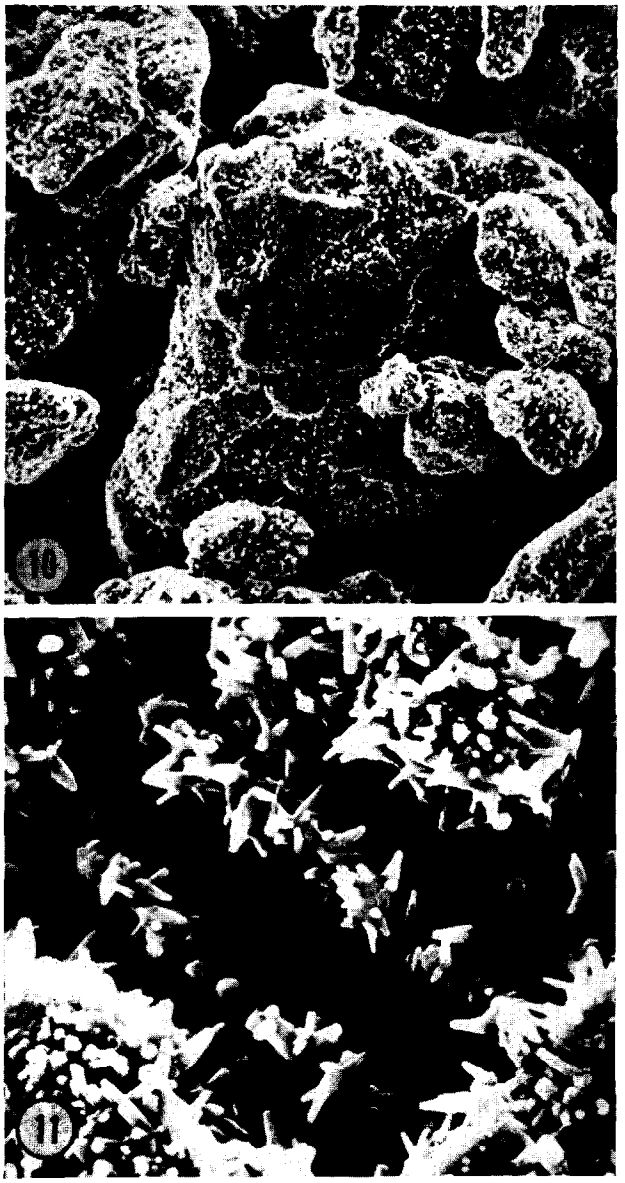

FIG. 10. Scanning electron micrographs (Figs. 10–12 and 14–19): General view of a Type IVA catalyst grain; ca. 110×.

FIG. 11. Fissure in a Type IVA catalyst "decorated" with lath-like crystals; ca. 2220×.

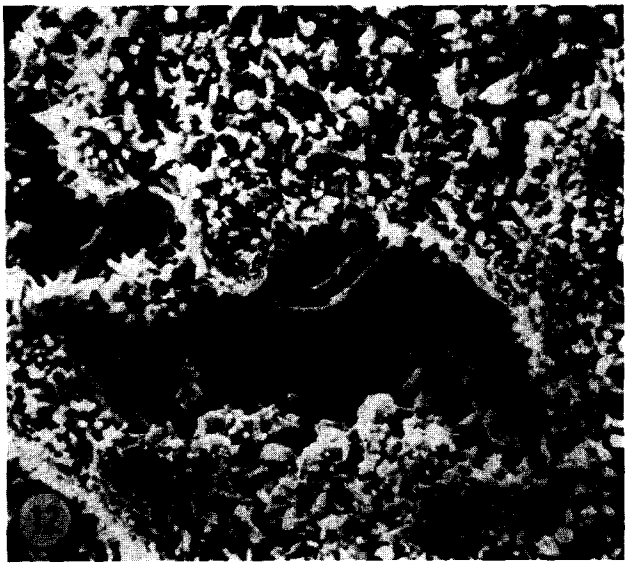

FIG. 12. Bridging of large fissures in Type IVA catalyst by lath-like crystals; ca. 1100×.

the suggestion that alumina trihydrates covers surface areas and pore volumes larger than their own (*6*).

ACKNOWLEDGMENTS

The authors acknowledge gratefully fellowship funds provided by the Davison Chemical Company; and thank Dr. F. G. Ciapetta, Dr. T. H. Cheavens, and N. E. Miller for helpful discussions.

REFERENCES

1. KOKES, R. J., AND EMMETT, P. H., *J. Amer. Chem. Soc.* **81,** 5032 (1959).
2. MARS, P., SCHOLTEN, J. J. F., AND ZWIETERING, P., *Acetes Congr. Int. Catal. 2nd, 1961* **1,** 1245 (1961).
3. ROBERTSON, S. D., AND ANDERSON, R. B., *J. Catal.* **23,** 286 (1971).
4. YASUMURA, J., *Nature (London)* **173,** 80 (1954).
5. KNAPPWOST, A., AND MADER, K. H., *Naturwissenschaften* **52,** 590 (1965).
6. FREEL, J., PIETERS, W. J. M., AND ANDERSON, R. B., *J. Catal.* **14,** 247 (1969).
7. FREEL, J., PIETERS, W. J. M., AND ANDERSON, R. B., *J. Catal.* **16,** 281 (1970).
8. FREEL, J., ROBERTSON, S. D., AND ANDERSON, R. B., *J. Catal.* **18,** 243 (1970).
9. OATLEY, C. W., NIXON, W. C., AND PEASE, R. F. W., *Advan. Electron. Electron Phys.* **21,** 181 (1965).
10. THORNTON, P. R., "Scanning Electron Microscopy." Chapman and Hall, London, 1968.
11. PEASE, R. F. W., BROERS, A. K., AND PLOC, R., *Proc. Eur. Conf. Elec. Micros., 3rd, Prague* **1,** 389 (1964).
12. REIMSCHUSSEL, A. M., AND FREDERICKS, R. J., *J. Mater. Sci.* **4,** 885 (1969).
13. HIRSCH, P. B., HOWIE, A., NICHOLSON, R. B., PASHLEY, D. W., AND WHELAN, M. J., "Electron Microscopy of Thin Crystals," pp. 295–316. Butterworths, London, 1965.
14. RUDEE, M. L., *Carbon (Oxford)* **5,** 155 (1967).
15. AVERY, N. R., AND SANDERS, J. V., *J. Catal.* **18,** 129 (1970).
16. ENNOS, A. E., *Brit. J. Appl. Phys.* **4,** 401 (1933).
17. LIPPENS, B. C., PhD thesis, Delft, 1961.
18. OOMES, L. E., DE BOER, J. H., AND LIPPENS, B. C., *Proc. Int. Symp. Reactiv. Solids, 4th,* 1960, 317 (1961).
19. COENEN, J. W. E., PhD thesis, Delft, 1958.
20. HAINE, M. E., AND EINSTEIN, P. A., *Proc. Eur. Conf. Elec. Micros., 2nd, Delft* **1,** 97 (1960).

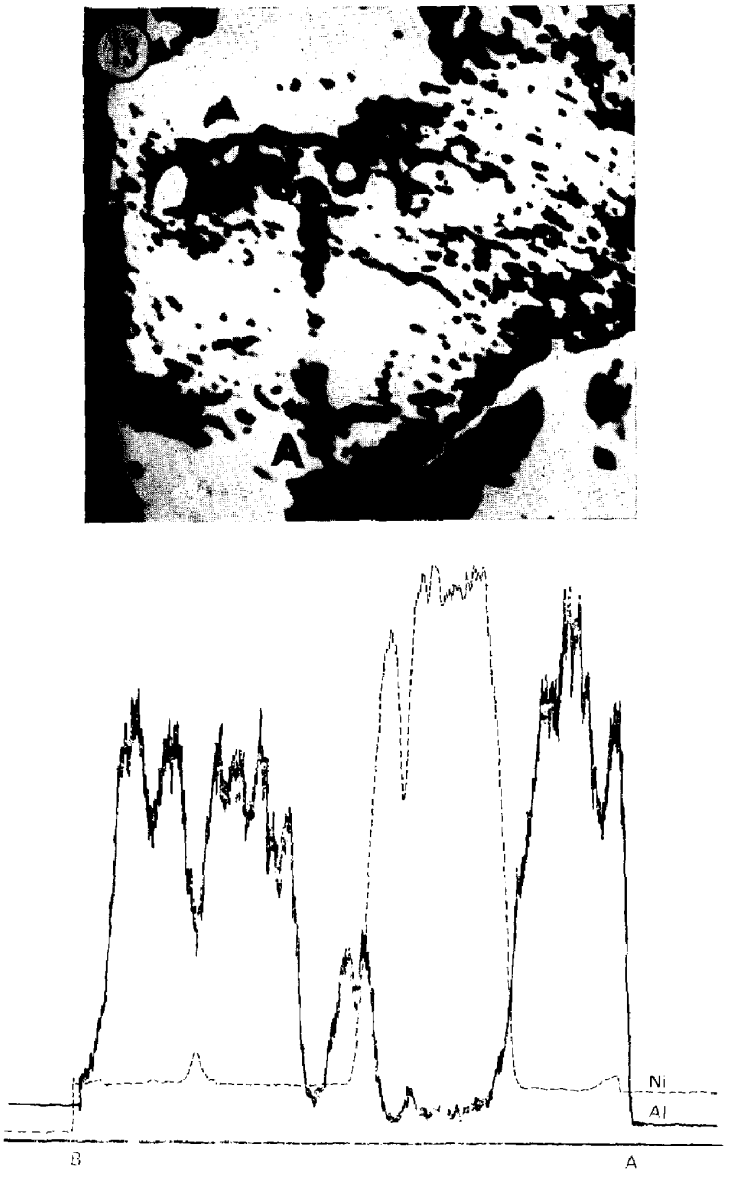

FIG. 13. Ratemeter outputs of nickel K-α (attenuation = 4000 counts/sec) and aluminum (attenuation = 400 counts/sec) radiation by scanning from point A to point B on a Type IVA catalyst grain under the beam of an electron-probe microanalyzer. Maximum nickel signals correspond to a minimum in the aluminum and vice versa.

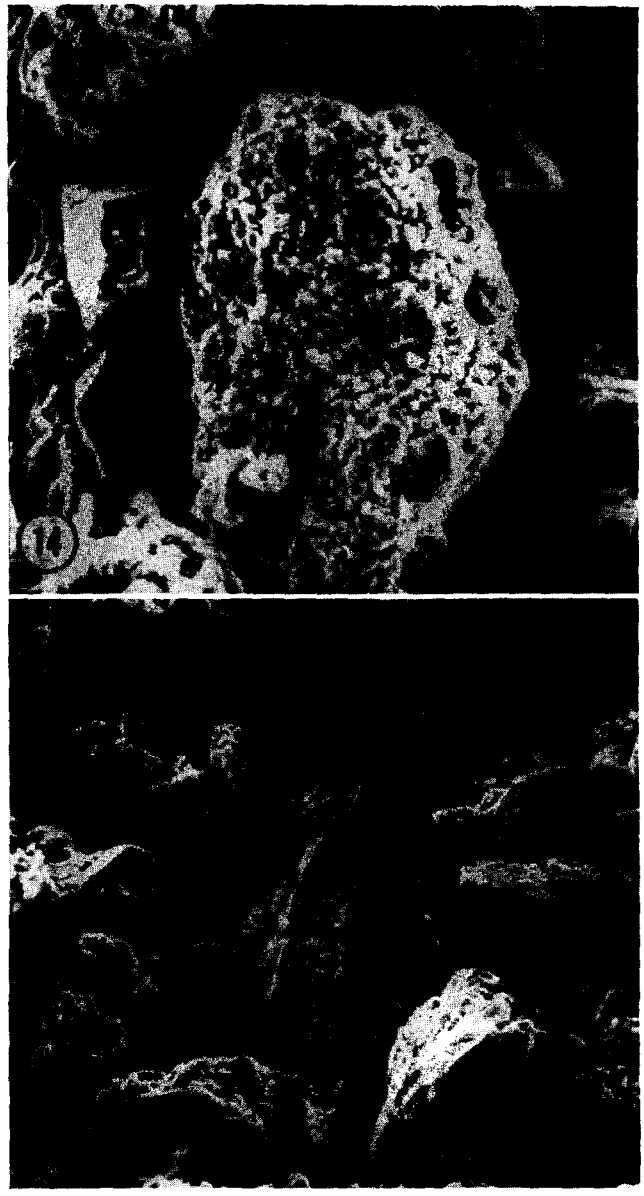

FIG. 14. Type IVA catalyst + 2 hr/50°C/20% NaOH. Morphology of covering layer becomes more rounded; 550×.

FIG. 15. Type IVA catalyst + 2 hr/50°C/20% NaOH showing extensive exposure of nickel surface; ca. 220×.

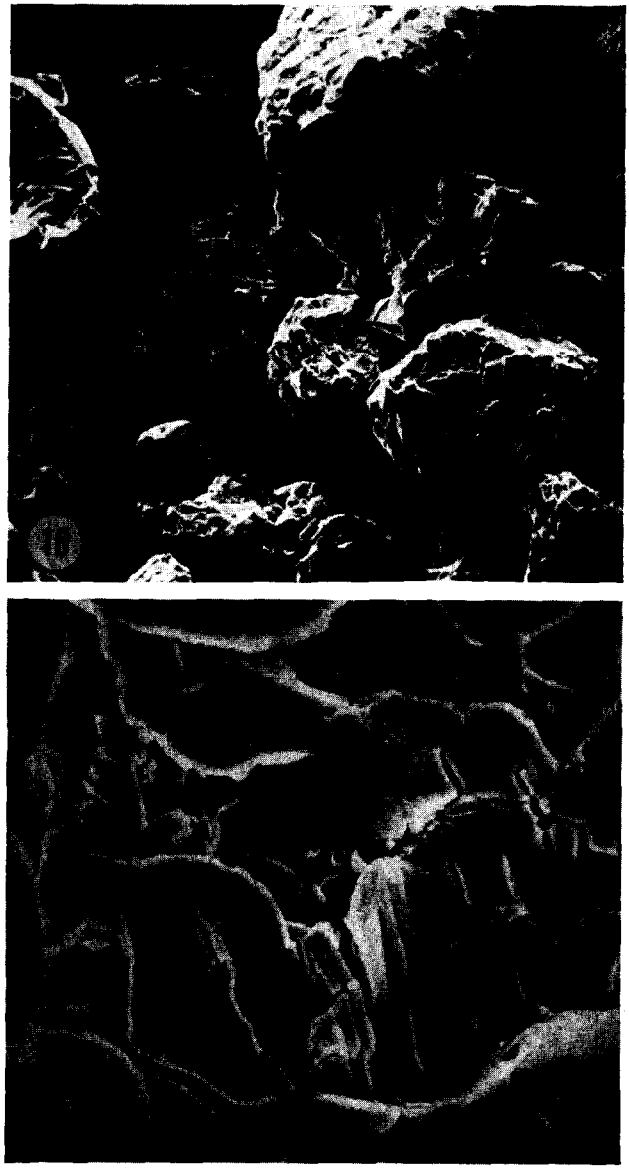

FIG. 16. General view of Type IIA catalyst; ca. 1100×.
FIG. 17. Fissure zones in Type IIA catalyst with residual particulate material, ca. 1100×.

FIG. 18. General view of Type $IIIA_1$ catalyst; ca. 220×.
FIG. 19. Wide fissure zones in Type $IIIA_1$ catalyst with residual particulate material; ca. 2200×.